LASER & PHOTONICS REVIEWS

www.lpr-journal.org

Arbitrary Phase Access for Stable Fiber Interferometers

Piotr Roztocki, Benjamin MacLellan, Mehedi Islam, Christian Reimer, Bennet Fischer, Stefania Sciara, Robin Helsten, Yoann Jestin, Alfonso Cino, Sai T. Chu, Brent Little, David J. Moss, Michael Kues, and Roberto Morandotti**

Well-controlled yet practical systems that give access to interference effects are critical for established and new functionalities in ultrafast signal processing, quantum photonics, optical coherence characterization, etc. Optical fiber systems constitute a central platform for such technologies. However, harnessing optical interference in a versatile and stable manner remains technologically costly and challenging. Here, degrees of freedom native to optical fibers, i.e., polarization and frequency, are used to demonstrate an easily deployable technique for the retrieval and stabilization of the relative phase in fiber interferometric systems. The scheme gives access (without intricate device isolation) to $<1.3 \times 10^{-3}$ π rad error signal Allan deviation across 1 ms to 1.2 h integration times for all tested phases, ranging from 0 to 2π. More importantly, the phase-independence of this stability is shown across the full 2π range, granting access to arbitrary phase settings, central for, e.g., performing quantum projection measurements and coherent pulse recombination. Furthermore, the scheme is characterized with attenuated optical reference signals and single-photon detectors, and extended functionality is demonstrated through the use of pulsed reference signals (allowing time-multiplexing of both main and reference signals). Finally, the scheme is used to demonstrate radiofrequency-controlled interference of high-dimensional time-bin entangled states.

1. Introduction

Interferometers mediate the superposition of electromagnetic fields to produce interference patterns. In one of the most common configurations used—known as the Michelson scheme (**Figure 1**a)—light is split into two equal-energy beams by a beam-splitter. Following propagation and reflection, the spatial modes recombine and interfere on the beam-splitter, with the light intensity at each of the splitter outputs dependent on the relative optical phase, determined by the path length traveled by the two beams (i.e., the interferometer imbalance). Length differences smaller than optical wavelengths (e.g., <2000 nm for the infrared wavelengths used in telecommunications) have perceivable impacts on the recombined light's output intensity, and thus the coherent mixing of beams has strict stability requirements. Optical beam-mixing operations hold relevance in both the history and the cutting edge

P. Roztocki, B. MacLellan, M. Islam, Dr. C. Reimer, B. Fischer, Dr. S. Sciara, R. Helsten, Dr. Y. Jestin, Prof. M. Kues, Prof. R. Morandotti
Institut National de la Recherche Scientifique (INRS-EMT)
Varennes, QC, Canada
E-mail: michael.kues@iop.uni-hannover.de; morandotti@emt.inrs.ca

P. Roztocki, Dr. Y. Jestin
Ki3 Photonics Technologies
Montreal, QC, Canada

Dr. C. Reimer
HyperLight Corporation
Cambridge, MA, USA

Dr. S. Sciara, Prof. A. Cino
Department of Engineering
University of Palermo
Palermo, Italy

The ORCID identification number(s) for the author(s) of this article can be found under https://doi.org/10.1002/lpor.202000524

DOI: 10.1002/lpor.202000524

Prof. S. T. Chu
Department of Physics and Material Science
City University of Hong Kong
Hong Kong, China

Prof. B. Little
State Key Laboratory of Transient Optics and Photonics, Xi'an Institute of Optics and Precision Mechanics
Chinese Academy of Science
Xi'an, China

Prof. D. J. Moss
Optical Sciences Centre
Swinburne University of Technology
Hawthorn, VIC, Australia

Prof. M. Kues
Institute of Photonics
Leibniz University of Hannover
Hannover, Germany

Prof. R. Morandotti
Institute of Fundamental and Frontier Sciences
University of Electronic Science and Technology of China
Chengdu, China

of physics, e.g., in fundamental studies of light transport,[1] the characterization of optical coherence properties of light sources,[2–4] scaling laser power,[5] as well as classical and quantum signal processing and communications;[6–9] thus, stable interferometric systems are critical, ubiquitous tools to modern science.

While the sensitivity of interferometers to small perturbations predicates their widespread use for metrology, it is a detriment when used for coherent signal processing: unintentional perturbations (e.g., mechanical, seismic, thermal effects) easily couple to the interferometer and, thus, to the beam-mixing procedure (Figure 1a). Without proper treatment, these errors can reduce interference contrasts and in extreme cases, render interferometers inoperable (Figure 1b)—an issue that is exasperated when several interferometers/operations are concatenated, which limits the complexity/scalability of signal processing. Being able to distinguish a signal from such perturbations, accurately reconstruct the interferometer phase, and/or actively stabilize this phase (in real time or in post-compensation) is the basis of most applications. In free-space interferometers, where the beams propagate through air or vacuum, over a century of development has produced numerous solutions for phase reconstruction; these include arm dithering,[10,11] adding auxiliary active and passive optical elements into the arms,[12] using multiple spatial paths per arm,[13,14] as well as complex and expensive isolation infrastructure and light sources.[15] The basis of many of these methods is the so-called "quadrature condition," that refers to the use of two reference signals whose interference responses are offset from one another by $\frac{\pi}{2}$ (e.g., a sine and a cosine response). Thus, when one signal is at a minimum in sensitivity to perturbation, the other signal is at a maximum. This enables a linear, phase-independent response to perturbations.[12,13,16,17] However, free-space interferometers are generally neither durable, compact, nor mass-producible—characteristics required by the demanding frontiers of established and emerging applications (e.g., technologies deployed as part of telecommunications grids[18,19] and space-borne instrumentation[20,21]). The technological maturity of fiber optics should allow to address these requirements, to access large length scales (inaccessible to integrated photonics[22]) in a compact footprint, and to enable practical, widespread interferometry. Moreover, fiber plays a central role in the quantum telecommunications infrastructure. Fiber interferometric systems are particularly critical for time-based data manipulation (e.g., executing projection measurements on time-bin-encoded states using imbalanced interferometers[23–26]) with reduced coupling losses versus, e.g., fiber-to-chip coupling. However, stability and full phase control are not easily achievable in fiber interferometric systems, currently limiting their potential use.

In particular, many free-space components or already-developed interferometer designs do not have accessible counterparts in fiber and generally, deployed optical fiber systems suffer from larger phase drifts. Several works towards reconstructing and stabilizing phase in fiber interferometers have thus been introduced,[27–33] featuring impressive milestones accomplished through diverse experimental approaches. These include, for example, the injection of single-frequency reference lasers,[27] variants of the Pound–Drever–Hall method,[32] modulation of an interferometer arm,[29–31,33] and explorations of weak references for phase reconstruction.[28,34] However, present phase-retrieval

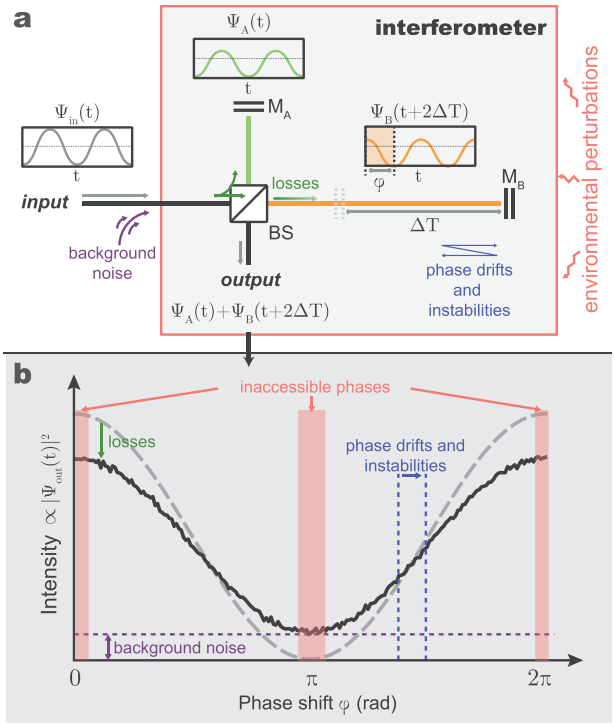

Figure 1. Role of optical phase in the operation of an interferometer. a) Schematic of a standard unbalanced interferometer, here a Michelson-type commonly used in coherent signal processing. An electromagnetic wave, $\Psi_{in}(t)$ (gray), enters the input port of a beam-splitter (BS), where it is reflected/transmitted into two, length-unbalanced arms (spatial modes). Here, the resulting fields are described by Ψ_A (solid green line) and Ψ_B (solid orange line), respectively. Following reflection at the terminating mirrors (M_A, M_B) and recombination on the BS, a summed wave, $\Psi_{out}(t)$, is emitted from the two BS output ports (here, only one is shown for simplicity). As the relative phase difference between the two arms varies, the intensity of $\Psi_{out}(t)$ oscillates sinusoidally—the signature effect of interferometers. Note that for clarity, constant phase shifts arising from, e.g., the BS are not depicted. b) Environmental perturbations and non-idealities couple to the operation of the interferometer and degrade the ideal high-contrast interference (dashed gray line). In practice (solid black line): 1) optical losses and background events reduce interference contrast (i.e., visibility); 2) interferometer phase drifts and instabilities may distort the fringes; and 3) not all interferometric phases may be accessible/resolvable (depending on the interferometer phase-reconstruction method used). Phases inaccessible for stabilization using single-color reference-based schemes (see also Figure 4) are illustrated here.

schemes address some interferometer requirements while compromising others. These include: 1) introducing ambiguities in the reconstructed phase (due to phase-to-feedback mappings that are not one-to-one[27,28]); 2) making certain interferometer phases inaccessible for stabilization, or accessible but at the cost of limited resolution or robustness[27–29] (e.g., by sweeping interferometer delay or optical reference frequency to follow high-derivative interference points); 3) demanding increased setup complexities, footprints, and costs (requiring, e.g., additional radiofrequency routing,[29,32] intricate vibration isolation and temperature controls,[35] dithering of an interferometer arm[10,29,31,33]); and 4) introducing noise background photons[10,27,29,31,32] (originating from bright stabilization lasers or their nonlinear/Rayleigh scattering). In

a recent, impressive demonstration in the context of quantum telecommunications,[34] a phase drift of 19.63 rad ms^{-1} was post-compensated by probing the interferometric system phase at microsecond rates by means of weak pulse trains with alternating, orthogonal (0 or $\frac{\pi}{2}$) phase encodings. It is, however, expected that in deployed conditions, much faster phase drifts will have to be tracked, demanding further investigation into the constraints of such coherent-state recovery schemes.

Here, targeting this context of phase compensation in fiber interferometric systems, we characterize (using both bright and dim/photon-level beams) a phase-recovery method that makes use of quadrature encoding in degrees of freedom well-suited for inexpensive manipulation and propagation in optical fiber, and with a particular suitability towards quantum optics. We study the use of continuous wave (CW) and pulsed reference signals, showing that the latter has the potential to enable increased quantum signal-to-noise ratios via the temporal multiplexing of the signal and reference. Furthermore, we prepare high-dimensional time-bin entangled quantum states (i.e., the discrete form of energy–time entangled states[36] with more than two levels) by making use of a stabilized pulsed laser and integrated microcavity. Then, using interferometers stabilized with our method, we demonstrate quantum interference via an atypical degree of freedom: the carrier-envelope offset (CEO) radiofrequency. Our work thus supports the readiness of our scheme for advanced use cases, especially in quantum photonics.

2. Results

Presently, a common inexpensive stabilization technique relies on coupling a reference CW laser into the interferometer and measuring the interfered signal (I_x, **Figure 2**a). This signal varies as a cosine ($I_x(\varphi) = I_{\text{mid}}[1 + V\cos(\varphi)]$, where the intensity $I_{\text{mid}} = \frac{I_{\max}+I_{\min}}{2}$ and V is the interference visibility) and is used to extract the interferometer phase φ.[27] While experimentally straightforward relative to the current state-of-the-art, such a single-color approach is limited since several phases between 0 and 2π correspond to the same intensity (that is, the map from intensity to phase is not one-to-one in this range, e.g., $\varphi = \frac{\pi}{2}, \frac{3\pi}{2}$ both map to I_{mid}). This leads to ambiguities in phase retrieval, typically requiring the active sweeping of the laser wavelength or the interferometer delay,[27,29] making it difficult to reproduce phase settings, or to lock multiple interferometers to different phases with a single source. However, as the optical frequency of such an injected signal is changed (e.g., via an acousto-optic modulator), its cosine response is shifted in phase. This means that a slightly offset optical frequency component is sufficient to output a $\frac{\pi}{2}$-shifted, sine response relative to I_x (i.e., the quadrature signal, I_y, Figure 2a). Phase ambiguity is present when only I_x is acquired, but can be eliminated by measuring simultaneously the orthogonal signals I_x and I_y. When acquired together, I_x and I_y map one-to-one to a phase between 0 and 2π (Figure 2b), allowing for the unambiguous retrieval of the interferometer phase (see Experimental Section). A very small optical frequency offset between the two injected signals is required to maintain a similar period of I_x and I_y. For example, for a portable interferometer with a 4 ns imbalance in the telecom band at 1550 nm,[9,36] a frequency offset of 188 MHz can be used (see Experimental Section). However, most off-the-shelf filters cannot separate such finely spaced frequencies for the simultaneous measurement of the two interferences. Towards this end, we exploit the polarization degree of freedom—easily controlled and propagated with minimal cross-talk in fiber optics—to prepare a reference signal where I_x and I_y travel in orthogonal polarization modes of the fiber (Figure 2c and Experimental Section). The two-color reference signal is prepared from one source, which is split into a passive and an acousto-optic modulated arm to create the frequency-shifted, orthogonally polarized, I_x and I_y components. This reference signal is fed into the interferometer. Once it is interfered and output, an off-the-shelf fiber polarization beamsplitter (rather than an expensive, custom-made filter) is used to split the two frequencies for detection of the intensities I_x and I_y.

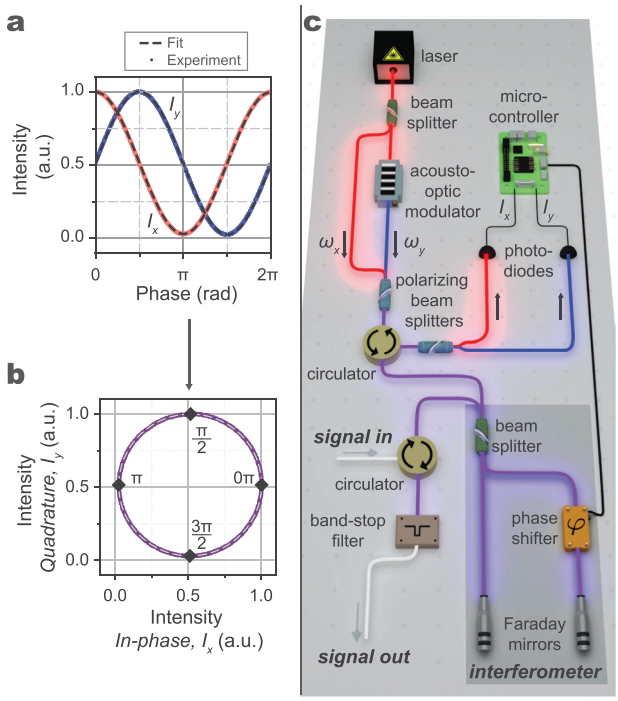

Figure 2. Retrieving fiber interferometer phase using a two-color reference signal. a) A two-color (ω_x and ω_y) optical signal, created from a single source (see main text), is injected into an interferometer, with the ideal (dashed line) and experimental (acquired with photodiodes, red and blue markers) interference outputs I_x and I_y shown as a function of the interferometer phase (referenced at ω_x, see Experimental Section). ω_y was chosen such that I_x and I_y are out of phase by $\frac{\pi}{2}$. The use of such a reference signal enables an unambiguous, one-to-one map between the experimental coordinate pair $\{I_x, I_y\}$ and the interferometer phase φ in the range $[0,2\pi)$. This is evidenced in (b) depicting the relation of I_y and I_x (Lissajous pattern, with ellipse fit overlaid). c) Scheme of the setup, experimentally realized using off-the-shelf telecommunications components, with the two parts of the reference prepared to propagate on orthogonal fiber polarizations. This enabled straightforward separation of the two finely spaced reference frequencies ω_x and ω_y at the detection stage (using only a polarizing beam-splitter rather than expensive filters) for phase extraction and stabilization. In parallel, an input signal under test co-propagates in the unbalanced interferometer (built to provide an 11.5 ns imbalance). As the frequency difference between the signal under test and the reference signal can be chosen to be on the order of hundreds of gigahertz, they can be easily separated by using an off-the-shelf, band-stop filter.

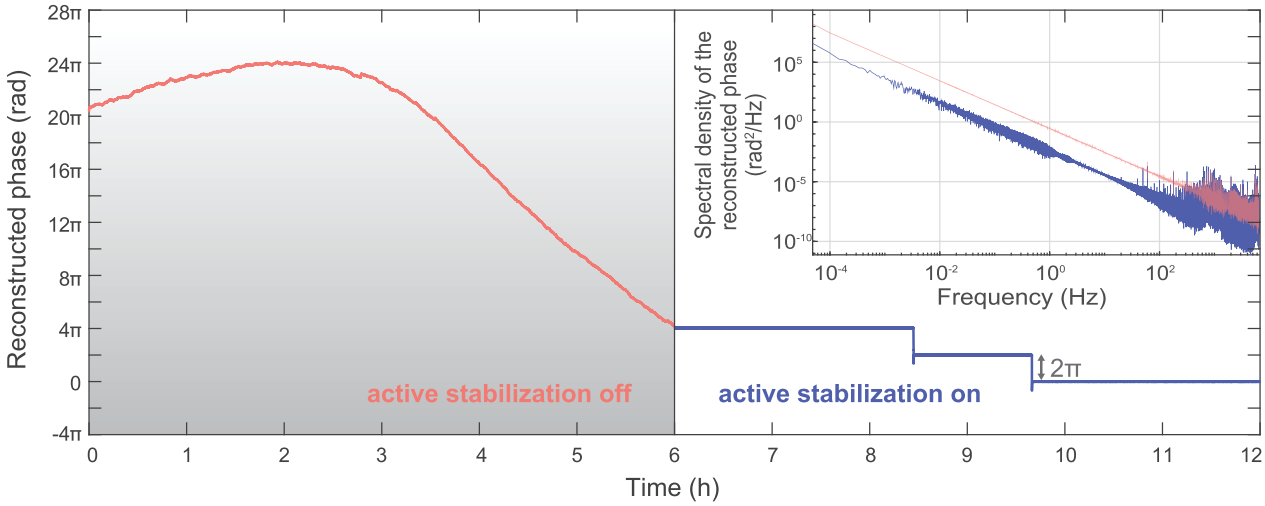

Figure 3. Long-term interferometric phase stability. Phase drift in a fiber interferometer reconstructed in-loop from our error signal without (left) and with (right) active phase recovery and feedback. When the fiber-stretcher/digital-to-analog converter voltage limits are reached, the target phase is preserved by the stabilization algorithm enacting a fast, cyclic shift of 2π (see step-like transitions on the right). Such long-term stability is particularly important for long measurements, e.g., those related to quantum state tomography. Inset: Spectral density of the reconstructed phase (see Experimental Section) in the presence (blue) and absence (red) of active stabilization, demonstrating an order of magnitude reduction in phase change for most spectral components, particularly the low and intermediate frequencies currently accessible with the speed of our feedback loop.

Note also that this signal can be prepared once and distributed among several interferometers, providing a common reference.

With the additional use of passive stabilization methods (mechanical damping), perturbations were limited to frequencies below tens of kilohertz. Consumer-grade, portable digital electronics were then easily integrated into the system for phase retrieval and real-time correction (see Experimental Section; similarly, low-footprint electronics can also provide the AOM driving signal), with on-the-fly phase tunability via a fiber stretcher in one of the arms. Tracking and compensating for fluctuations enables long-term phase stability (relative to our reference, i.e., measured in-loop, **Figure 3**), as required for many measurements with long integration times and common optical references (e.g., quantum state characterization). Alternatively, without real-time stabilization, if our reference signal is tracked through the duration of a measurement, the phase could be post-compensated/post-selected. Such interferometric phase-tracking schemes for post-compensation are already used in several application domains.[37–39]

An issue in phase-recovery schemes based on the use of a single interference signal (without sampling an orthogonal component) is that phase perturbations are not equally resolvable across all phases. This limits the range of accessible interferometric phase values, unless, e.g., the reference laser frequency or interferometer delay is actively tuned to follow sensitivity maxima,[27,29] which however, introduces issues of setup complexity and reduced reproducibility. Looking at the example of a single-color reference signal (which, while not the most advanced, has a low experimental complexity comparable to our method), the response of the feedback signal to phase changes (the so-called system "sensitivity") is described by $S \propto |\frac{\mathrm{d}I_x}{\mathrm{d}\varphi}| = |VI_{\mathrm{mid}}\sin(\varphi)|$. The sensitivity, and by proxy the accuracy of phase retrieval (relative to the optical reference), can be seen to be extremely phase dependent, with minima at the 0 and π phases. This restricts the range of phases accessible using such a feedback signal (**Figure 4**a). Instead, using our two-colored feedback signal, comprising the in-phase and quadrature components, makes the sensitivity constant for all phases, as $S \propto |\frac{\mathrm{d}(I_x+iI_y)}{\mathrm{d}\varphi}| = |-VI_{\mathrm{mid}}\sin(\varphi) + iVI_{\mathrm{mid}}\cos(\varphi)| = VI_{\mathrm{mid}}$. As a result, all phases $[0,2\pi)$ are individually accessible (Figure 4a) with phase-independent stabilization performance (Figure 4b). This is demonstrated even more directly via Allan error signal deviation analysis for different integration times (Figure 4c and Experimental Section). Moreover, we observe an Allan deviation of 5.89×10^{-5} π rad (in-loop, equivalent to 0.04 nm at 1550 nm optical wavelength) at an integration time of 2:11 min (and even at integration times of 1 h 9 min, this value remains below 1×10^{-3} π rad). This value outperforms most other implementations in the state of the art (see Table S1, Supporting Information), and is also unique in its practical, inexpensive, real-time stabilization.

Several fields that require coherent optical processing can benefit from our scheme: quantum optical state processing constitutes an application with some of the most strict and demanding requirements. Specifically, our scheme gives access to long integration times for photon signals, and unambiguous, uniform stability across all phase projection measurements. These are required for complete quantum state characterization (tomography), high-visibility quantum interference, and repeatable quantum operations—measurements demonstrated (using our scheme for real-time stabilization) in the context of recent 2D and high-dimensional time-bin entanglement works.[9,40,41]

Further supporting the quantum use case for our scheme, we show the radiofrequency-controlled quantum interference of high-dimensional time-bin entangled states prepared using an integrated source, see **Figure 5**. It is important to note that while our past measurements using this stabilization scheme[9,23] exploited a common optical reference across both state preparation and characterization stages, for this measurement we

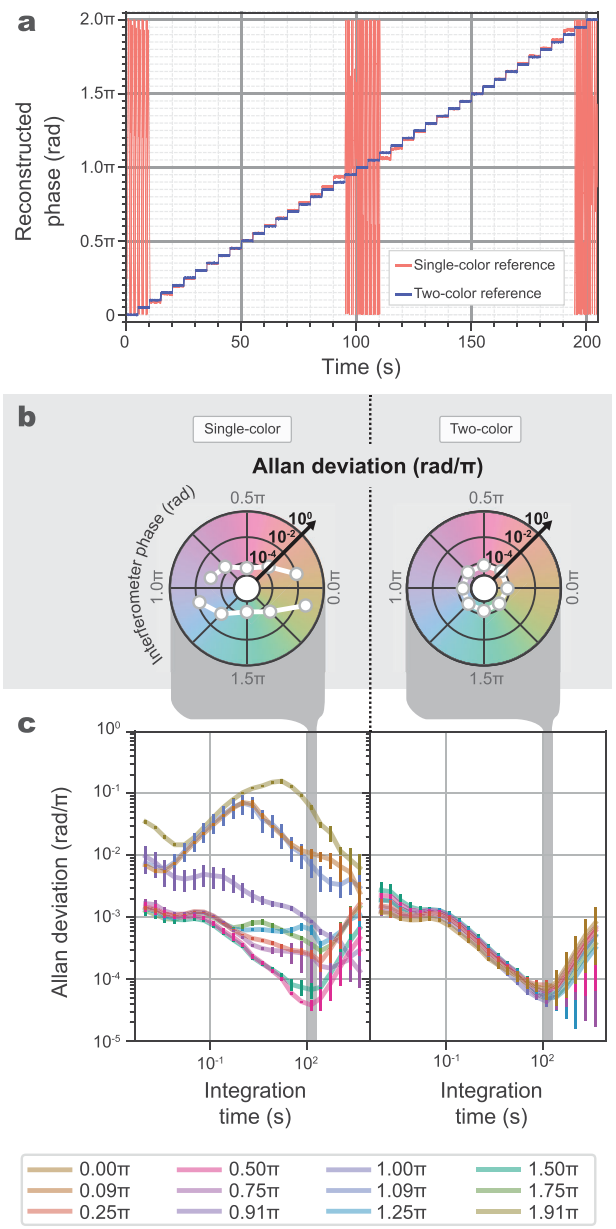

Figure 4. Use of the two-color reference signal enabling phase-independent interferometer stabilization. a) The interferometric phase is stabilized from 0 to 2π in steps of 0.05 π, using both single-color (red) and two-color (blue) phase-stabilization algorithms (see Experimental Section) in the feedback loop. The single-color feedback system is unable to stabilize at the minima points of its sensitivity ($\{0,\pi\}$) and has an increasing error when approaching these points. In contrast, the two-color feedback system has stable access to all phases in the range $[0,2\pi)$ while maintaining a similarly low setup complexity. b) System phase stabilization as a function of the target interferometer phase (plotted in polar coordinates, with a logarithmic radial axis). The points correspond to the Allan error signal deviation value at an integration time of 131 s (vertical gray bar in (c)). The single-color method (left) demonstrates a decrease in stability approaching its sensitivity minima at 0 and π, while the two-color method (right) has a largely uniform stability across all phases in the $[0,2\pi)$ range. c) Allan deviation analysis of the phase error signal (see Experimental Section) over a range of integration times. While the two-color stabilization (right) shows near-identical in-loop stability between all target phases, the single-color Allan deviation magnitudes vary greatly between phases. As use independent optical sources for state preparation (a pulsed, commercial frequency comb source) and interferometer stabilization (a separate, i.e., out-of-loop, CW source with low frequency jitter). In particular, the frequency comb's parameters are stabilized with respect to atomically referenced, tunable radiofrequencies (as part of a turn-key MENLO system, see Experimental Section). When this pulsed excitation is used to prepare a time-bin entangled state (as a pump source), the phase encoded in the qubits linearly corresponds to the pulse-to-pulse phase θ_{CEO};[9,23,42] thus, such radiofrequencies (particularly the CEO frequency reference, which defines θ_{CEO}[43]) may be important degrees of freedom for, e.g., quantum optical metrology.[44] Using this comb source for the excitation of signal-idler photon pairs, together with the independent CW source to stabilize the interferometer phase at 0π (Figure 5a), we show that the CEO radiofrequency is an accessible degree of freedom to demonstrate quantum interference (Figure 5b,c). We note that the associated interference periodicity depends on whether the interferometer arm length corresponds to 1× or 2× the repetition rate, i.e., a delay of 4 or 8 ns in our case (Figure 5c). The potential use of such low-power interference measurements for the stabilization and perhaps the direct extraction of mode-locked laser CEO frequencies bears further investigation. The successful demonstration of quantum interference using independent optical sources for the pump and interferometer reference (albeit with very high stability metrics, see Experimental Section) also suggests that constraints in future quantum experiments may be relaxed.

A number of quantum photonics experiments and technologies demand minimal background photon counts, which bright stabilization lasers (in wavelength regions near the quantum signal bands) and limited filtering cannot always provide, bringing about nonnegligible cross-talk. We investigate two directions that may resolve this issue for such delicate application cases. First, we implement a heavy attenuation of the bichromatic CW reference signal (prior to injection into the interferometer) to produce a few-photon interference response (measured using single-photon detectors, see **Figure 6**a). This is an attractive solution, as the low-power probe signal no longer requires high rejection filters, meaning even off-the-shelf DWDM (dense wavelength division multiplexing) filters can reduce cross-talk. Such attenuated coherent states have been investigated for interferometer phase reconstruction[45] and experimentally demonstrated in a single-color stabilization scheme to lock on one phase.[28] Here, we extend these efforts and investigate the use of two attenuated coherent states in quadrature for phase-retrieval. Measuring the in-phase and quadrature signal outputs at one interferometer port (Figure 6a), we illustrate the trade-off, brought about by the Poissonian statistics governing coherent states, between the phase estimation error and the signal integration time (i.e., better phase estimation for longer integration times and higher reference signal powers, see Experimental Section). These statistics give rise to a phase dependence in the phase estimation error (Figure 6b, a dependence removed when both output ports are

the single-color retrieval could not be stabilized at 0 and π, measurements were instead performed at $\pm 0.09\pi$ of these points. Error bars correspond to the standard deviation calculated from three measurements.

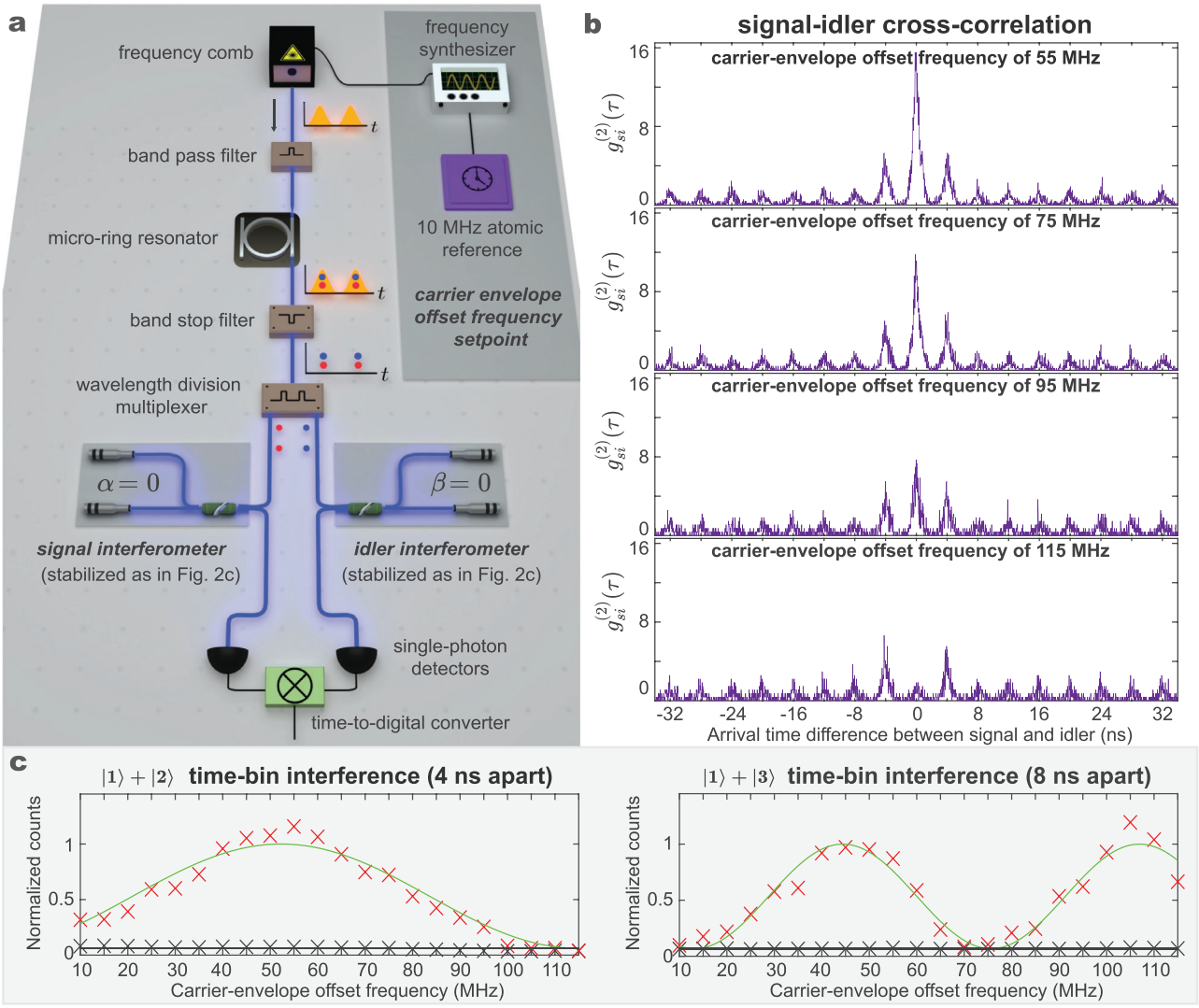

Figure 5. Quantum interference of time-bin entangled photons generated via a stabilized frequency comb source. a) A frequency comb is used to excite a single resonance of an integrated microcavity to generate time-bin entangled photon pairs via spontaneous four-wave mixing.[9] The signal and idler are then split and interfere in fiber interferometers stabilized (using our scheme) on a constant, zero phase. The coincidence between the two channels is then measured and correlated using single-photon detectors and time-tagging electronics. The frequency comb repetition rate and carrier-envelope frequencies are both stabilized with respect to a Rubidium reference clock. As the CEO frequency setpoint (given by a radiofrequency tone) is swept, quantum interference is observed in the coincidence events (b). Projections on $|1\rangle + |2\rangle$ versus $|1\rangle + |3\rangle$ are made available by switching the interferometer arm fibers to access different length imbalances (4 and 8 ns respectively, corresponding to 1× and 2× the frequency comb pulse period). The CW laser used to stabilize the two interferometers is not referenced or locked to the frequency comb or atomic reference—the two sources are independent (i.e., out-of-loop). c) Quantum interference measurements for the time-bin encoded photon states, accomplished by sweeping the CEO frequency of the comb source. The raw visibilities for the interference between quantum time-bins one and two periods apart are, in this case, 88.4% and 87.3%, respectively (without any locking of the pump and reference lasers).

used). For experiments where these detriments can be tolerated in exchange for reduced cross-talk, we append a heat map illustrating the trade-off between these parameters (Figure 6c). In practice, the integration time should be chosen so that the fastest phase drifts can be resolved. The count rate will be limited by the saturation point of the detectors used, the maximum power available from the optical reference, or the maximum power allowed that still minimizes cross-talk to acceptable boundaries.

Second, the stabilizing laser in the scheme does not have to be CW (CW references produce background noise photons over all detection time windows). Mode-locked sources (and especially stabilized frequency combs, see Experimental Section) have sufficient coherence lengths to produce interference signals (**Figure 7**a), a characteristic already exploited in the context of classical optics[46] as well as quantum communications,[34] and here implemented with our I_x/I_y reference scheme. In the context of quantum optics, the use of these pulsed sources allows new functionalities for interferometric systems. In particular, when a pulsed laser is used within our scheme as a reference, its induced photon background becomes limited to distinct

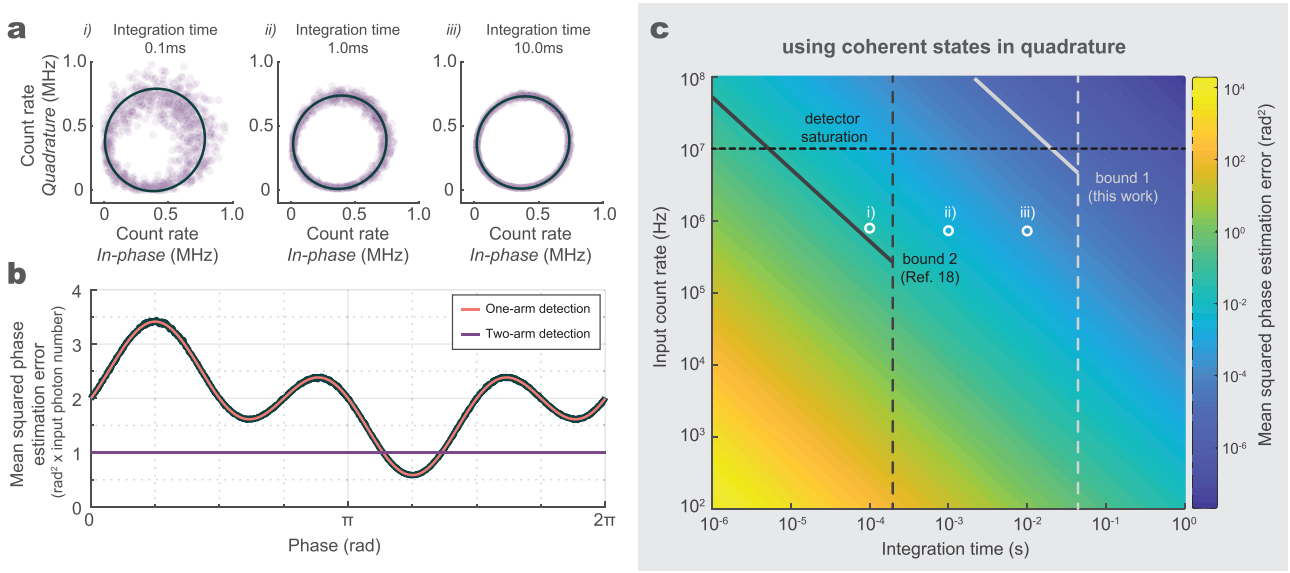

Figure 6. Experimental considerations for interferometer phase estimation using attenuated coherent states. a) Photon count rates for the in-phase and quadrature channels, measured with two single-photon detectors as the interferometer phase is swept. Increasing the signal integration time shows an increase in phase estimation accuracy. b) The phase dependence of the estimation error for this method, arising from the Poissonian statistics governing coherent states, determined analytically (red curve, see Experimental Section) and from the average of 10 000 Monte Carlo simulations (black curve). c) Average phase estimation error as a function of photon flux and integration time. The maximum phase drift rate, maximum allowable phase error, and single-photon detector saturation rate are the key parameters for deciding the experimental values of count rate and integration time to be used. We denote two example bounds: bound 1, based on the data corresponding to our interferometer system (our system's detector saturation rate is also illustrated), and bound 2, based on data from a recent work making use of a 275 km fiber interferometric system[18] (see Experimental Section). White markers indicate our expected performance with the three integration times demonstrated in (a).

temporal modes that can be delayed with respect to the quantum input being interfered. This background can then either be suppressed via time-gating, or post-selected in analysis. A fast photodiode can then be used to track the phase from pulse to pulse or otherwise, a slower photodiode can effectively integrate over the signal if simpler electronics are required (Figure 7a). Reducing resource requirements further, the pulsed reference can be attenuated to the few-photon level (alike to Figure 6) and the in-phase and quadrature components of the feedback signal can be temporally delayed with respect to one another (via a tunable fiber imbalance on the AOM arm). Such an approach, which resembles temporally interleaved quadrature sampling techniques from the field of digital signal processing,[47,48] allows us to retrieve the interferometer phase information using only one single-photon detector (Figure 7b). While requiring less infrastructure, the non-simultaneous measurement of the in-phase and quadrature signals will give rise to a phase-dependent error in the phase reconstruction, brought about by phase drifts between these samples (Figure 7c; such small errors are negligible for most applications, we note, e.g., the maximum phase drift νT is <10 mrad in a recent literature example[34]), on top of the aforementioned noise contributions arising from Poissonian photon statistics. These analyses generalize to any coherent states in quadrature used for phase reconstruction (i.e., also in degrees of freedom alternative to polarization). As coherent-state phase-retrieval techniques of this type have recently been introduced into the context of quantum communications,[34] these considerations may be of use for extending such systems to realizations deployed out-of-lab (where faster phase drifts will have to be compensated).

3. Conclusion

In closing, we have realized a practical and accessible scheme for the unambiguous retrieval of phase in the fiber interferometer platform without the need to dither or sweep the stabilizing laser frequency, demonstrating long-term stability, access to all phase values, as well as new interference control variables. We have additionally characterized the use of the scheme with dim reference beams, presenting reduced background photon counts, and as well, we have analyzed operational considerations brought about by resource constraints. In extensions of the scheme, we expect that single-photon-level, quadrature-encoded reference signals may also find appropriate use cases where it is mandatory to avoid stimulated processes (e.g., high-power signals, complex photonic chips) or where minimal system disturbances are important (e.g., quantum ranging[49]). The method presented here is limited to unbalanced interferometer applications (as equal arm lengths cannot provide the required phase-offset in reference components, making other schemes[12] more suitable for balanced interferometer stabilization); it is not suited for use with reference lasers with unstable optical powers unless forced calibration steps or algorithmic upgrades are included (in contrast to, e.g., methods based on minimizing dither tones[29]); and it is best suited towards Michelson-like configurations, as extending our method to others, e.g., the Mach–Zehnder, would require supplementary polarization control. Future work on this method will focus on further increasing stability and phase resolution through the use of higher bit-depth and faster electronics (see Experimental Section), performing out-of-loop stability

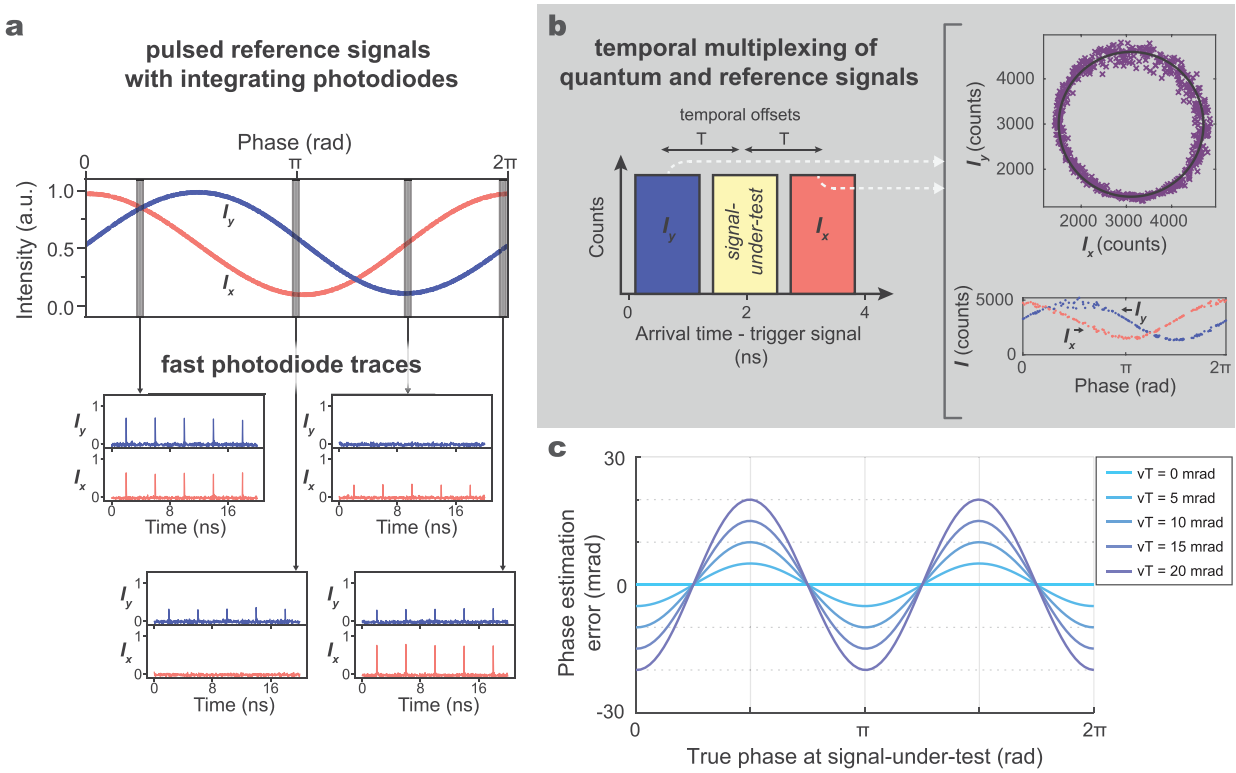

Figure 7. Interferometry with a pulsed optical reference in quadrature. a) Slow (2.1 kHz, top) and fast (50 GHz, bottom) photodiode traces of the interferometer output when a frequency comb laser is used in the scheme (Figure 2c). Importantly, the interferometer arm difference is matched to the laser repetition rate (or its multiple). The signals I_x and I_y then maintain orthogonality and continue to allow unambiguous phase retrieval, while confining reference-induced background photon counts to specific time windows. b) Use of an attenuated pulsed reference. The in-phase and quadrature signals can be offset by a time T (here with a delay line) with respect to processed quantum inputs to increase their signal-to-noise ratio. Here, we offset a signal under test with respect to the pulsed references, and feed it into a single, triggered photon-detector. We find that the reference background maintains orthogonality, meaning a single detector can retrieve both a signal under test and its corresponding phase mapping. c) The error in reconstructed phase induced when the in-phase and quadrature signals are measured at times $+T$ and $-T$ relative to the signal under test, respectively, and in the presence of a linear phase drift rate ν.

measurements using additional optical sources and longer fibers (determining scheme appropriateness beyond coherent signal processing), extending the scope of the demonstrated scheme to interferometers with more arms (as required for, e.g., high-dimensional state manipulation without cascading two-arm interferometers), as well as to integrated interferometers.[50,51]

4. Experimental Section

CW Reference Signal Preparation: The reference signal was a low-frequency jitter CW source (NKT Koheras BASIK E15, 1550 nm central wavelength, 40 mW optical power, <2 kHz bandwidth, coherence length above 47.7 km ≫ the maximum 2.3 m interferometer imbalance (equivalent to 11.5 ns) used in the measurements). Half of the output was used as the I_x signal component, while the other half was frequency up-shifted by δf using an acousto-optic modulator (Brimrose TEMF-200-40-30-1500-2FP) driven by an RF synthesizer (Tektronix AWG701B) and RF amplifier (Kune Electronic Microwave Components KU-PA-BB-005250-2A) to produce the I_y signal component. In order to satisfy the orthogonality criterion for the two components, the RF signal amplitude was adjusted to provide near-equal interference amplitudes for I_x and I_y, and δf was made equal to $\frac{c}{(4n_g \cdot \Delta L)}(2n+1)$, where c is the speed of light in vacuum, n_g is the effective group index of refraction, ΔL is the total length imbalance between the two interferometer paths, and n is an integer (kept as small as possible to ensure comparable periodicity between I_x and I_y). As the length imbalance (or equivalently, the relative time delay) of the demonstrated interferometer was 11.5 ns (and 4/8 ns for Figure 5), the δf in the experiments was 196 MHz (and 188/218 MHz)—chosen to suit the bandwidth of our acousto-optic modulator. I_x and I_y were then made to co-propagate in a single fiber but on orthogonal polarization axes through the use of a 2 × 1 polarizing beam-splitter—the I_x and I_y components were then injected into the fiber interferometer. The fibers used in the reference signal preparation were all polarization-maintaining (for added environmental stability), while the interferometer was composed of single-mode fibers (mechanically dampened with steel plates). Faraday mirrors in the interferometer compensate for birefringence effects experienced during propagation.

Signal Acquisition and Phase Reconstruction: The reference signal interferes at the interferometer beam-splitter, the two arms having experienced a relative phase shift of $\varphi = 2\pi n_g \cdot \Delta L \cdot f/c$, where f is the frequency of the input light (thus each of the two colors acquires a different phase). The two colors were then split apart at the output using a polarizing beam-splitter, and the two intensities I_x and I_y were acquired using two photodiodes (Thorlabs PDA50B, 235 kHz bandwidth). The phase was then reconstructed (relative to the optical reference) using

$$\varphi = \arctan 2\left[\frac{2I_y - I_y^{\max} - I_y^{\min}}{I_y^{\max} - I_y^{\min}}, \frac{2I_x - I_x^{\max} - I_x^{\min}}{I_x^{\max} - I_x^{\min}}\right] \quad (1)$$

where arctan2 is the two-argument arctangent function, while I^{max} and I^{min} correspond to the interference maxima and minima, respectively.

For the case of a single-color reference (Figure 4), the I_x signal was used on its own to probe the interferometer phase. The phase was then reconstructed as $\varphi = \arccos\left[2(I_x - I_x^{min})/(I_x^{max} - I_x^{min}) - 1\right]$. Generally, this method can only stabilize phase values in the range $(0,\pi)$;however, we stabilized on target phases in the $(\pi,2\pi)$ range by inverting the sign of the feedback signal. This single-color stabilization was accomplished with no physical changes to the setup, only modifying the phase stabilization algorithm in the feedback loop.

Phase Stabilization Feedback Loop: In this realization, the photodiode voltage outputs were fed into a microcontroller (Arduino Due, 12-bit analog-to-digital converter, 12-bit digital-to-analog converter, 84 MHz clock rate), which then reconstructed the interferometer phase φ in real time using these signals (see phase reconstruction above). The associated error $\epsilon = \varphi^* - \varphi$, from the target phase φ^*, was then used as the feedback signal in a proportional–integral–derivative feedback loop to adjust a fiber-stretcher-based phase shifter (General Photonics, FPS-001, maximum bandwidth 20 kHz—note the feedback signal was limited in speed to fit this bandwidth) placed in one of the interferometer arms. All presented data were collected by monitoring I_x and I_y with a separate analog-to-digital converter (National Instruments DAQ System, models PCI 6251+BNC2090, 16-bit analog-input, 1.0 MS s^{-1} aggregate sampling rate) and acquisition computer, with these signals being subsequently used to reconstruct the phase using Equation (1).

Frequency-Domain Analysis of Long-Term Stabilization: In the inset of Figure 3, the spectral characteristics of the reconstructed phase, $\varphi(t)$ (calculated from the reference interference signals I_x and I_y), were analyzed. The phase signal was extracted using Equation (1) and phase-unwrapped. The spectral density of the reconstructed interferometer phase signal is proportional to $|F(\varphi(t))|^2$, and is normalized by the measurement bandwidth, where F is the one-sided Fourier transform. The inset of Figure 3 displays the average spectral density of four reconstructed phase signals.

Allan Deviation Measurements: In Figure 4b,c, the stability of the reconstructed phase was evaluated using the Allan deviation, a metric first introduced in the context of clocks/frequency references and that describes the stability of the interferometric phase over different time scales.[52,53] Here, we used the Allan deviation expression given by

$$\sigma(\tau) = \sqrt{\frac{1}{2M}\sum_{m=1}^{M-1}\left(\bar{\varphi}_{m+1} - \bar{\varphi}_m\right)^2} \tag{2}$$

where $\bar{\varphi}$ is the average of $\varphi(t)$ over an integration time τ, with m being an index of consecutive averages, and $M = m\tau$. At short integration times, averaging removes high-frequency fluctuations in the interferometer phase signal. However, above ≈100 s integration time, the system reaches a noise floor where the noise is dominated by non-stationary noise sources, such as random walk and drift, causing an increase in the Allan deviation.[54] This noise is likely caused by power drifts in the reference signal, which can lead to drifts away from the initial system calibration.

CEO Frequency Control of Quantum Interference: The setup was changed to that in Figure 5a. Here, a stabilized frequency source (Menlo FC1500-250-WG, 250 MHz repetition rate) was used to excite a single resonance of a nonlinear microcavity to generate time-bin entangled photon pairs (namely, signal, and idler) described by the quantum state $|1\rangle_s|1\rangle_i + e^{i\theta}|2\rangle_s|2\rangle_i + e^{i2\theta}|3\rangle_s|3\rangle_i$, where $|k\rangle$ $(k = 1,2,3)$ denote a time-bin quantum state and "s" and "i" denote the signal and idler photon, respectively. Here, the pulse to pulse phase θ is described by $\frac{2\pi f_{CEO}}{f_{rep}}$ where f_{CEO} corresponds to the CEO frequency (sweepable via a radiofrequency input into the Menlo system), and f_{rep} corresponds to the pulse repetition rate (here, set constant to 250 MHz). Both the signal and idler interferometer phases were kept constant at 0 rad (relative to a CW-based reference signal), θ was then swept by changing the radiofrequency input over an accessible range of 10–115 MHz. After exiting the interferometers, the photons impinged onto two independent detectors (Quantum Opus) and time-tagging electronics (Picoquant Hydraharp). The quantum interference was then computed by post-selecting the interfered time-bin for the two channels, cross-correlating these counts to determine the second-order correlation function (g^2_{si}, Figure 5b), and then fitted with a Glauber function and a Gaussian (signal and background, respectively) to determine the normalized counts. Note that, as described above, the laser sources used for state preparation and interferometer stabilization were independent, and demonstrated a maximum relative frequency drift rate of ≈270 kHz h^{-1}, corresponding to a $<0.01\pi$ rad h^{-1} interferometer drift (which is negligible relative to the total 2 h integration time for each of our quantum interference measurements).

Single-Photon Reference Signal Preparation and Measurement: For the attenuated-laser reference signal measurements in Figure 6, a polarization-maintaining variable optical attenuator was inserted immediately before the two-color reference signal was injected into the interferometer. The rest of the setup was kept the same as in Figure 2c, with the exception of the photodiodes replaced with two superconducting nanowire single-photon detectors (Quantum Opus, one for I_x and one for I_y), connected to time-tagging electronics (Picoquant Hydraharp). For Figure 6a, the fiber stretcher in the interferometer arm was then swept, and the photon arrival times at each channel collected. A moving integration window was then implemented in post-selection to determine both the count rates and the integration-time response of the system.

Figure 6b,c, presents the analysis of the phase estimation errors introduced by a quadrature-based reference using coherent states, which follow Poissonian statistics. The mean photon number of each quadrature channel is $\bar{n}_x = \frac{\bar{n}}{2}(1 + V\cos(\varphi))$ and $\bar{n}_y = \frac{\bar{n}}{2}(1 + V\sin(\varphi))$, where V is the interference visibility, $\bar{n}$ is the input mean photon number, and each channel has variance $\Delta n_{x,y}{}^2 = \bar{n}_{x,y}$. Propagating this variance through Equation (1), the mean squared phase error is (Figure 6b, solid red line)

$$\Delta\varphi^2_{est} = \frac{2}{V^2\bar{n}}\left(1 + V\sin(\varphi)\cos^2(\varphi) + V\sin^2(\varphi)\cos(\varphi)\right) \tag{3}$$

which scales in agreement with the standard quantum limit.[28,45] If, instead, both output arms of the interferometer were monitored using a difference detection scheme (i.e., the corresponding reference signals at each output arm are subtracted from each other), this phase-dependent error is removed and $\Delta\varphi^2_{est} = \frac{1}{V^2\bar{n}}$ (Figure 6b, solid purple line). However, such monitoring requires increased costs and complexity as two additional single-photon detectors are needed.

Experimentally, the mean photon number is the product of the detector integration time, τ, and the photon flux rate, Φ, both of which may be bounded by implementation considerations (Figure 6c) such as the maximum phase drift velocity present (ν), detector saturation rate, or maximum permissible phase estimation error ($\Delta\varphi_{max}$). For the bounds on integration time in Figure 6c, the definition that was used is $\tau \leq \Delta\varphi_{max}/\nu$. Bound 1 is based on data from the system presented in this work, i.e., $\Delta\varphi_{max} = \pi \times 10^{-3}$ rad (from Figure 4) and $\nu = 0.071$ rad s^{-1} (identified as the fastest phase drift in the unstabilized trace of Figure 3). Bound 2 is based on data from Lucamarini et al.[18] for an interferometric system with arm lengths of 275 km, with $\nu = 1.0$ rad ms^{-1} and assuming $\Delta\varphi_{max} = \pi/16$ (corresponding to half the phase slice size employed).

Pulsed Reference Signal Preparation and Measurement: This setup is identical to the one used with the CW reference (Figure 2c), but with the original laser source replaced with a stabilized frequency comb output (Menlo FC1500-250-WG, 250 MHz repetition rate) filtered down to a 200 GHz optical bandwidth using band-pass filters and amplifiers (Santec and Lightwave 2020, Pritel SPFA). For Figure 7a, the integrating photodiodes used (Thorlabs PDA50B, 2.1 kHz bandwidth acquired with the National Instruments DAQ System PCI 6251+BNC2090) were slow with respect to the signal repetition rate and acted as a signal integrator. On the other hand, the fast photodiodes (Finisar XPDV, 50 GHz bandwidth) were connected with a high-bandwidth oscilloscope to reproduce the pulse train interference (Agilent DSO-X 92804A, 28 GHz bandwidth, 80 GSa s^{-1}).

In the reference signal preparation (Figure 2c), the source was equally split into two different paths to introduce a frequency shift with the AOM

on one of them. Before recombination, an optical delay line is added to implement a relative time difference between I_x and I_y (Figure 7b). The injection of this temporally interleaved reference signal into the interferometer can then be adjusted with another delay line to enable time-multiplexing with the signal under test. The detector-triggered signal is provided by the frequency comb pulse train. In post-processing, the different temporal channels (Figure 7b) can then be easily separated to reconstruct the respective signals. The presented data were acquired for 120 s with an integration time of 100 ms (this corresponds to averaging over many sampling cycles).

Temporal offsets between I_x, I_y, and the signal under test introduce phase estimation errors (Figure 7c), as fast fluctuations in fiber length can impart different interferometric phases onto each of these components. To estimate the maximum error that could be introduced from such temporal interleaving, a maximum phase drift rate of ν that is changing linearly over the total reference time window was assumed. I_x and I_y are separated in time from the signal under test by $+T$ and $-T$, respectively, with measured intensities $I_x(\varphi + \nu T)$ and $I_y(\varphi - \nu T)$. When comparing the phase estimated from these shifted reference signals (using Equation (1)) and the interferometer phase at the signal under test (φ), a phase-dependent error arises (Figure 7c). For small values of νT, the maximum observed error is equal to νT; however, as this product increases, the maximum error begins to scale nonlinearly and the phase-dependent error plotted in Figure 7c becomes skewed.

Supporting Information

Supporting Information is available from the Wiley Online Library or from the author.

Acknowledgements

P.R. and B.M. contributed equally to this work. This work was supported by the Natural Sciences and Engineering Research Council of Canada (NSERC) through the Steacie, Synergy, Strategic, Discovery and Acceleration Grants Schemes, by the MESI PSR-SIIRI Initiative in Quebec, by the Canada Research Chair Program, and by the Australian Research Council Discovery Projects scheme (DP150104327). P.R. and C.R. acknowledge the support of NSERC Vanier Canada Graduate Scholarships. B.M. acknowledges support provided by an NSERC CGS-M fellowship. M.K. acknowledges funding from the European Union's Horizon 2020 Research and Innovation programme under the Marie Sklodowska-Curie grant agreement number 656607. S.T.C. acknowledges support from the CityU APRC programme number 9610356. B.L. acknowledges support from the Strategic Priority Research Program of the Chinese Academy of Sciences (grant number XDB24030300). R.M. is affiliated to the Institute of Fundamental and Frontier Sciences as an adjoint professor. The authors thank J. Azaña for providing some of the required equipment and S. MacLean as well as H. Eisenberg for useful discussions. Special thanks go to Quantum Opus and N. Bertone of OptoElectronic Components for their continuous support and for providing state-of-the-art photon detection equipment.

Open access funding enabled and organized by Projekt DEAL.

Conflict of Interest

P.R. and Y.J. are involved in developing fiber interferometer products at Ki3 Photonics Technologies.

Data Availability Statement

The data that support the plots within this paper and other findings of this study are available from the corresponding authors upon reasonable request.

Keywords

interferometers, coherent signal processing, quantum photonics

Received: November 20, 2020
Revised: February 17, 2021
Published online: May 4, 2021

[1] A. Regensburger, C. Bersch, M.-A. Miri, G. Onishchukov, D. N. Christodoulides, U. Peschel, *Nature* **2012**, *488*, 167.
[2] J. M. Dudley, G. Genty, S. Coen, *Rev. Mod. Phys.* **2006**, *78*, 1135.
[3] R. Trebino, *Frequency-Resolved Optical Gating: The Measurement of Ultrashort Laser Pulses*, Springer US, Boston, MA **2000**.
[4] C. K. Hong, Z. Y. Ou, L. Mandel, *Phys. Rev. Lett.* **1987**, *59*, 2044.
[5] T. Y. Fan, *IEEE J. Sel. Topics Quantum Electron.* **2005**, *11*, 567.
[6] W. Drexler, U. Morgner, R. K. Ghanta, F. X. Kärtner, J. S. Schuman, J. G. Fujimoto, *Nat. Med.* **2001**, *7*, 502.
[7] K. Kikuchi, in *High Spectral Density Optical Communication Technologies* (Eds: M. Nakazawa, K. Kikuchi, T. Miyazaki), Springer, Berlin **2010**, pp. 11–49.
[8] N. Gisin, R. Thew, *Nat. Photonics* **2007**, *1*, 165.
[9] C. Reimer, M. Kues, P. Roztocki, B. Wetzel, F. Grazioso, B. E. Little, S. T. Chu, T. Johnston, Y. Bromberg, L. Caspani, D. J. Moss, R. Morandotti, *Science* **2016**, *351*, 1176.
[10] A. A. Freschi, J. Frejlich, *Opt. Lett.* **1995**, *20*, 635.
[11] A. Dandridge, A. B. Tveten, T. G. Giallorenzi, *IEEE Trans. Microwave Theory Tech.* **1982**, *30*, 1635.
[12] G. Jotzu, T. J. Bartley, H. B. Coldenstrodt-Ronge, B. J. Smith, I. A. Walmsley, *J. Mod. Opt.* **2012**, *59*, 42.
[13] V. V. Krishnamachari, E. R. Andresen, S. R. Keiding, E. O. Potma, *Opt. Express* **2006**, *14*, 5210.
[14] D. Grassani, M. Galli, D. Bajoni, *Opt. Lett.* **2014**, *39*, 2530.
[15] LIGO Scientific Collaboration, *Phys. Rev. Lett.* **2016**, *116*, 061102.
[16] K. Liu, R. M. Measures, *J. Intell. Mater. Syst. Struct.* **1992**, *3*, 432.
[17] O. B. Wright, *Opt. Lett.* **1991**, *16*, 56.
[18] M. Lucamarini, Z. L. Yuan, J. F. Dynes, A. J. Shields, *Nature* **2018**, *557*, 400.
[19] E. Y. Zhu, C. Corbari, A. Gladyshev, P. G. Kazansky, H.-K. Lo, L. Qian, *J. Opt. Soc. Am. B* **2019**, *36*, B1.
[20] J. C. Chapman, T. M. Graham, C. K. Zeitler, H. J. Bernstein, P. G. Kwiat, arXiv:1901.07181 **2019**.
[21] R. Kaltenbaek, G. Hechenblaikner, N. Kiesel, O. Romero-Isart, K. C. Schwab, U. Johann, M. Aspelmeyer, *Exp. Astron.* **2012**, *34*, 123.
[22] C. Ma, W. D. Sacher, Z. Tang, J. C. Mikkelsen, Y. Yang, F. Xu, T. Thiessen, H.-K. Lo, J. K. S. Poon, *Optica* **2016**, *3*, 1274.
[23] C. Reimer, S. Sciara, P. Roztocki, M. Islam, L. Romero Cortés, Y. Zhang, B. Fischer, S. Loranger, R. Kashyap, A. Cino, S. T. Chu, B. E. Little, D. J. Moss, L. Caspani, W. J. Munro, J. Azaña, M. Kues, R. Morandotti, *Nat. Phys.* **2019**, *15*, 148.
[24] Y. Pilnyak, P. Zilber, L. Cohen, H. S. Eisenberg, *Phys. Rev. A* **2019**, *100*, 43826.
[25] F. Steinlechner, S. Ecker, M. Fink, B. Liu, J. Bavaresco, M. Huber, T. Scheidl, R. Ursin, *Nat. Commun.* **2017**, *8*, 15971.
[26] S. J. Nowierski, N. N. Oza, P. Kumar, G. S. Kanter, *Phys. Rev. A* **2016**, *94*, 042328.
[27] S.-B. Cho, T.-G. Noh, *Opt. Express* **2009**, *17*, 19027.
[28] D. Pulford, C. Robillard, E. Huntington, *Rev. Sci. Instrum.* **2005**, *76*, 063114.
[29] P. Toliver, J. M. Dailey, A. Agarwal, N. A. Peters, *Opt. Express* **2015**, *23*, 4135.
[30] H. Guo, A. Gnanapandithan, Y. Liu, C. Zhou, Z. Zheng, Y. Ou, X. Zeng, L. Qian, *J. Lightwave Technol.* **2019**, *37*, 1310.

[31] M. Song, S. Yin, P. B. Ruffin, *Appl. Opt.* **2000**, *39*, 1106.
[32] S. Rogers, D. Mulkey, X. Lu, W. C. Jiang, Q. Lin, *ACS Photonics* **2016**, *3*, 1754.
[33] H. Martin, X. Jiang, *Opt. Lett.* **2010**, *35*, 655.
[34] X.-T. Fang, P. Zeng, H. Liu, M. Zou, W. Wu, Y.-L. Tang, Y.-J. Sheng, Y. Xiang, W. Zhang, H. Li, Z. Wang, L. You, M.-J. Li, H. Chen, Y.-A. Chen, Q. Zhang, C.-Z. Peng, X. Ma, T.-Y. Chen, J.-W. Pan, *Nat. Photonics* **2020**, *14*, 422.
[35] M. Wada, S. Okubo, K. Kashiwagi, F. L. Hong, K. Hosaka, H. Inaba, *IEEE Trans. Instrum. Meas.* **2019**, *68*, 2246.
[36] J. Brendel, N. Gisin, W. Tittel, H. Zbinden, *Phys. Rev. Lett.* **1999**, *82*, 2594.
[37] X. Ma, M. Razavi, *Phys. Rev. A: At., Mol., Opt. Phys.* **2012**, *86*, 062319.
[38] B. J. Vakoc, S. H. Yun, J. F. de Boer, G. J. Tearney, B. E. Bouma, *Opt. Express* **2005**, *13*, 5483.
[39] D. Loterie, S. Farahi, D. Psaltis, C. Moser, *Proc. SPIE* **2015**, *9335*, 93350I.
[40] M. Kues, C. Reimer, P. Roztocki, L. R. Cortés, S. Sciara, B. Wetzel, Y. Zhang, A. Cino, S. T. Chu, B. E. Little, D. J. Moss, L. Caspani, J. Azaña, *Nature* **2017**, *546*, 622.
[41] M. Kues, C. Reimer, J. M. Lukens, W. J. Munro, A. M. Weiner, D. J. Moss, R. Morandotti, *Nat. Photonics* **2019**, *13*, 170.
[42] J. D. Franson, *Phys. Rev. Lett.* **1989**, *62*, 2205.
[43] A. M. Weiner, *Ultrafast Optics*, Wiley, Hoboken **2009**.
[44] N. Picqué, T. W. Hänsch, arXiv:1906.03706 **2019**.
[45] P. R. Saulson, *Fundamentals of Interferometric Gravitational Wave Detectors*, World Scientific, Singapore **2017**.
[46] K.-N. Joo, S.-W. Kim, *Opt. Express* **2006**, *14*, 5954.
[47] J. Howard, H. Landgraf, *Rev. Sci. Instrum.* **1994**, *65*, 2130.
[48] J. Saniie, M. Luukkala, *J. Phys. E: Sci. Instrum.* **1983**, *16*, 606.
[49] D. G. England, B. Balaji, B. J. Sussman, *Phys. Rev. A* **2019**, *99*, 023828.
[50] F. Ceccarelli, S. Atzeni, A. Prencipe, R. Farinaro, R. Osellame, *J. Lightwave Technol.* **2019**, *37*, 4275.
[51] H. Wang, J. Qin, X. Ding, M.-C. Chen, S. Chen, X. You, Y.-M. He, X. Jiang, L. You, Z. Wang, C. Schneider, J. J. Renema, S. Höfling, C.-Y. Lu, J.-W. Pan, *Phys. Rev. Lett.* **2019**, *123*, 250503.
[52] D. W. Allan, *Proc. IEEE* **1966**, *54*, 221.
[53] M. Mičuda, E. Doláková, I. Straka, M. Miková, M. Dušek, J. Fiurášek, M. Ježek, *Rev. Sci. Instrum.* **2014**, *85*, 083103.
[54] J. Jurado, C. M. Schubert Kabban, J. Raquet, *Navigation* **2019**, *66*, 251.